

Schwarzschild and Ledoux are equivalent on evolutionary timescales

EVAN H. ANDERS,^{1,2} ADAM S. JERMYN,^{3,2} DANIEL LECOANET,^{1,4,2} ADRIAN E. FRASER,^{5,2} IMOGEN G. CRESSWELL,^{6,2} AND
J. R. FUENTES⁷

¹*CIERA, Northwestern University, Evanston IL 60201, USA*

²*Kavli Institute for Theoretical Physics, University of California, Santa Barbara, CA 93106, USA*

³*Center for Computational Astrophysics, Flatiron Institute, New York, NY 10010, USA*

⁴*Department of Engineering Sciences and Applied Mathematics, Northwestern University, Evanston IL 60208, USA*

⁵*University of California, Santa Cruz, Santa Cruz, California 95064, U.S.A*

⁶*Department Astrophysical and Planetary Sciences & LASP, University of Colorado, Boulder, CO 80309, USA*

⁷*Department of Physics and McGill Space Institute, McGill University, 3600 rue University, Montreal, QC H3A 2T8, Canada*

(Received July 28, 2021; Revised October 19, 2021; Accepted; Published)

Submitted to ApJ

ABSTRACT

In stars, the location of convective boundaries is determined by either the Schwarzschild or Ledoux criterion, but there is not consensus among the 1D stellar modeling community over which criterion to use. In this letter we present a 3D hydrodynamical simulation of a convection zone whose boundary is stabilized by a composition gradient despite being thermally unstable. This convective boundary is Ledoux stable but Schwarzschild unstable. Over hundreds of convective overturn timescales, mixing at the convective boundary causes the convection zone to grow. The convection zone stops growing once it reaches a height where its boundary is stable by the Schwarzschild criterion. This work provides 3D evidence that convective boundaries which are Ledoux stable are fragile unless they are also Schwarzschild stable. Therefore, the Schwarzschild stability criterion properly describes the size of a convection zone, except for when convection zones do not reach statistically stationary states during short-lived evolutionary stages.

Keywords: Stellar convection zones (301), Stellar physics (1621); Stellar evolutionary models (2046)

1. INTRODUCTION

Observations tell us we don't understand the mixing at convective boundaries. For example, models and observations disagree about the sizes of convective cores (Claret & Torres 2018; Viani & Basu 2020; Pedersen et al. 2021), lithium abundances in solar-type stars (Pinsonneault 1997; Sestito & Randich 2005; Carlos et al. 2019; Dumont et al. 2021), and there is a well-known acoustic glitch in helioseismology at the base of the convection zone (see Basu 2016, Sec. 7.2.1). Improperly calculating the size of a convection zone can have important impacts across astrophysics such as setting the mass of stellar remnants (Farmer et al. 2019; Mehta et al. 2022)

and affecting the inferred radii of exoplanets (Basu et al. 2012; Morrell 2020).

While there are many undercertainties in convective boundary mixing (CBM), the most fundamental question is: what sets the nominal boundary of the CZ? One way of answering this question is by evaluating the *Schwarzschild criterion*, which determines where the temperature and pressure stratification within a star are stable or unstable. The other answer is the *Ledoux criterion*, which accounts for stability or instability due to the composition (e.g., the variation of helium abundance with pressure; see Salaris & Cassisi 2017, chapter 3, for a nice review of these criteria). Recent work states that these criteria are logically equivalent at a convective boundary in the mixing length formalism (Gabriel et al. 2014; Paxton et al. 2018, 2019), but they are not

always implemented to be that way (as in early versions of the MESA instrument, Paxton et al. 2013).

Modern studies still have not reached a consensus of which criterion to employ (see Kaiser et al. 2020, chapter 2, for a brief discussion). Multi-dimensional simulations have demonstrated that convection zones with Ledoux-stable boundaries expand by entraining compositionally-stable regions (Meakin & Arnett 2007; Woodward et al. 2015; Jones et al. 2017; Cristini et al. 2019; Fuentes & Cumming 2020; Androssy et al. 2020, 2021). However, it is unclear from past 3D simulations whether that entrainment should stop at a Schwarzschild-stable boundary, leading to uncertainty in how to model entrainment in 1D models (Staritsin 2013; Scott et al. 2021).

In this work, we present a simple 3D hydrodynamical simulation that demonstrates that convection zones with Ledoux-stable but Schwarzschild-unstable boundaries will entrain material over roughly a thermal timescale until both the Ledoux and Schwarzschild criteria are equivalent at the convective boundary. Therefore, in 1D stellar evolution models, when the evolution time is greater than or roughly equal to the thermal time (such as on the main sequence, see Georgy et al. 2021), these criteria should be implemented so that either one produces the same evolution. We briefly discuss these criteria in Sec. 2, display our simulations in Sec. ??, and provide a brief discussion in Sec. 4.

2. THEORY & EXPERIMENT

The stability of a convective region can instantaneously be determined using the Schwarzschild criterion,

$$\mathcal{Y}_S = \nabla_{\text{rad}} - \nabla_{\text{ad}}, \quad (1)$$

or the Ledoux criterion,

$$\mathcal{Y}_L = \mathcal{Y}_S + \frac{\chi_\mu}{\chi_T} \nabla_\mu \quad (2)$$

Here, the temperature gradient $\nabla \equiv d \ln P / d \ln T$ has a value of ∇_{ad} for an adiabatic stratification and ∇_{rad} if all flux is carried through radiative conductivity. The composition gradient $\nabla_\mu = d \ln \mu / d \ln P$ is multiplied by the ratio of $\chi_T = (d \ln P / d \ln T)_{\rho, \mu}$ and $\chi_\mu = (d \ln P / d \ln \mu)_{\rho, T}$, where ρ is the density, T is the temperature, P is the pressure, and μ is the mean molecular weight.

In Eqns. 1 and 2, \mathcal{Y} is the discriminant (e.g., Paxton et al. 2018, sec. 2), related to the superadiabaticity. In stellar structure codes, convective boundaries are assumed to coincide with sign changes in the discriminant. The various stability regimes which can occur in stars are well-described in section 3 and figure 3 of Salaris & Cassisi (2017), but we will briefly recap four important regimes:

1. Convection Zones (CZs): If $\mathcal{Y}_S > 0$ and $\mathcal{Y}_L \geq \mathcal{Y}_S$, a region's stratification is convectively unstable.
2. Radiative Zones (RZs): If both $\mathcal{Y}_S < 0$ and $\mathcal{Y}_L < \mathcal{Y}_S$, a region's stratification is stable to convection.
3. "Semiconvection" zone: If $\mathcal{Y}_S > 0$ but $\mathcal{Y}_L < 0$, a stable composition gradient stabilizes an unstable thermal stratification. These regions can be linearly unstable to overstable doubly diffusive convection (ODDC, see Garaud 2018, chapter 2), or they can be stable RZs.
4. "Thermohaline" zone: If $\mathcal{Y}_S < 0$ and $\mathcal{Y}_L > \mathcal{Y}_S$, a stable thermal stratification stabilizes an unstable composition gradient. These regions can be linearly unstable to thermohaline mixing or fingering convection (see Garaud 2018, chapter 3), or they can be stable RZs.

In this paper, we study 3D simulations of a linearly-stable semiconvection zone (#3) bounded below by a CZ (#1) and above by an RZ (#2). We examine how the boundary of the CZ evolves through entrainment. In particular, we are interested in seeing if \mathcal{Y}_S and \mathcal{Y}_L evolve towards the same height due to entrainment. Since stellar evolution timesteps generally span many convective overturn times, our 3D simulation should evolve to the proper state, which may be quite different from our initial conditions.

In this work, we utilize a simplified 3D model which employs the Boussinesq approximation, which assumes that the depth of the layer being studied is much smaller than the local scale height. Since we are studying thin regions near convective boundaries, this assumption is OK. The relevant physics for this problem are included (∇_{rad} varies with height, buoyancy is determined both by the composition C and the temperature stratification T), so \mathcal{Y}_S and \mathcal{Y}_L are meaningfully defined and distinct from one another when composition gradients are present. For details on our model setup and Dedalus simulations, we refer the reader to appendices A and B.

3. RESULTS

Volume visualizations of simulation dynamics are shown near the initial state (left) and evolved state (right) in Fig. 1. Buoyancy perturbations normalized by the vertical profile of buoyancy standard deviations are shown in the top two panels. Vertical velocity is shown in the bottom two panels. In the initial state, convection occurs in the bottom $\sim 1/3$ of the simulation domain; the middle $\sim 1/3$ of the domain is stabilized by a composition gradient, and the top $\sim 1/3$ is stabilized by a thermal gradient. The convection excites gravity waves

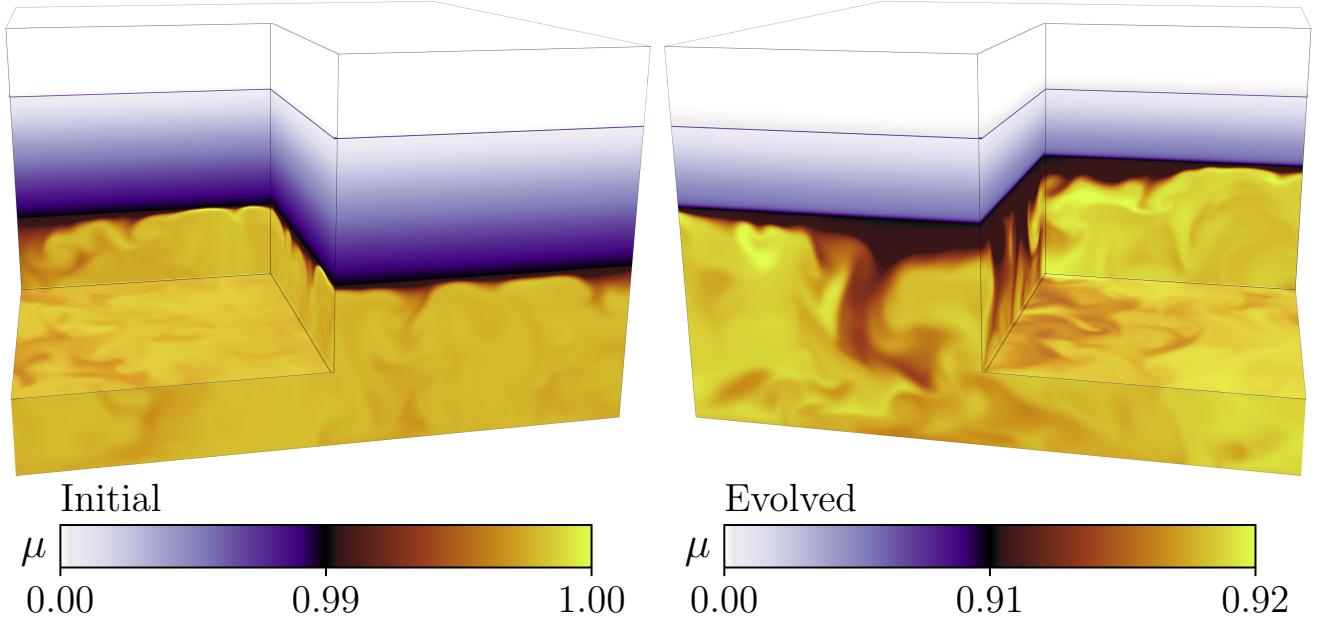


Figure 1. Volume renderings of the composition field in our simulations at early times (left) and late times (right); while our simulation domain spans $z = [0, 3]$, we only plot $z = [0, 2.5]$ here. We exaggerate the colorbar scaling in the convection zone (purple to yellow) to make convective mixing apparent. The purple gradient above the convection zone denotes the stable composition gradient, and the solid purple line denotes the bottom of the Schwarzschild stable region. Note that the evolved convection zone boundary (right) corresponds with the height of Schwarzschild stability. *Note: this is currently evolving further so that the last sentence isn't a lie.*

in the stable layers. The Brunt-Väisälä frequency is higher by a factor of 10 in the thermal layer than in the semiconvection layer, so the vertical velocity signature of motions there is smaller than in the semiconvection layer. Describe overshoot.

The most obvious difference between the panels on the left and the right is that the convection zone has grown in size from $\sim 1/3$ of the simulation domain to $\sim 2/3$ of the simulation domain. Through continuous overshoot, convection entrained stable, low-composition fluid from the upper region into the convection zone. This process eroded the composition gradient until the Schwarzschild and Ledoux boundaries of the convection zone were identical. In other words, the *thermal* stability of the upper zone is sufficient to halt expansion of the convection zone via entrainment, but compositional stability is not. We see negligible convective penetration (mixing of the buoyancy or entropy profile beyond the sign change in \mathcal{Y}), but this is expected and part of our experimental design (see appendix).

Figure 2 displays vertical profiles that have been averaged horizontally and in time. Profiles on the left show initial conditions, while profiles on the right show the evolved state. We show the composition (top panels), the Schwarzschild and Ledoux discriminants (mid-

dle panels), and the square Brunt-Väisälä and convective frequencies.

In the initial state, we see that the composition is uniform in the CZ ($z \leq 1$) and RZ ($z \geq 2$), but varies linearly in $z \in [1, 2]$ and provides stability. We also see that the sign change in \mathcal{Y}_L occurs at $z \sim 1$ while that in \mathcal{Y}_S occurs at $z \sim 2$. Finally, we see that $f_{\text{conv}} = 0$ because we initialize the simulation without any convective velocity. However, the Brunt-Väisälä frequency N^2 is negative in a boundary layer at the base of the CZ which drives the instability, and N^2 is stable above $z = 1$ (and is more stable by a factor of 10 above $z \sim 2$).

The final state (right) is attained after convection entrains and mixes through the initial composition gradient. We see that the composition profile (top) is constant in the convection zone, and approximates a step function above the CZ at the top of the overshoot zone. (TODO: Add overshoot to this figure). In this evolved state, the sign changes in the discriminants \mathcal{Y}_L and \mathcal{Y}_S coincide (middle panel). In the bottom panel, we see that the convective frequency is roughly constant, and see that $N^2 \lesssim 0$ in the bulk CZ. We can compute the “stiffness” $\mathcal{S} = N^2/f_{\text{conv}}^2$ of the radiative-convective boundary by comparing the average CZ value of $f_{\text{conv}}^2 \sim 10^{-2}$ to the RZ value of $N^2 \sim 10^2$, so $\mathcal{S} \approx 10^4$. Boundaries with a low stiffness $\mathcal{S} \lesssim 10$ easily deform in

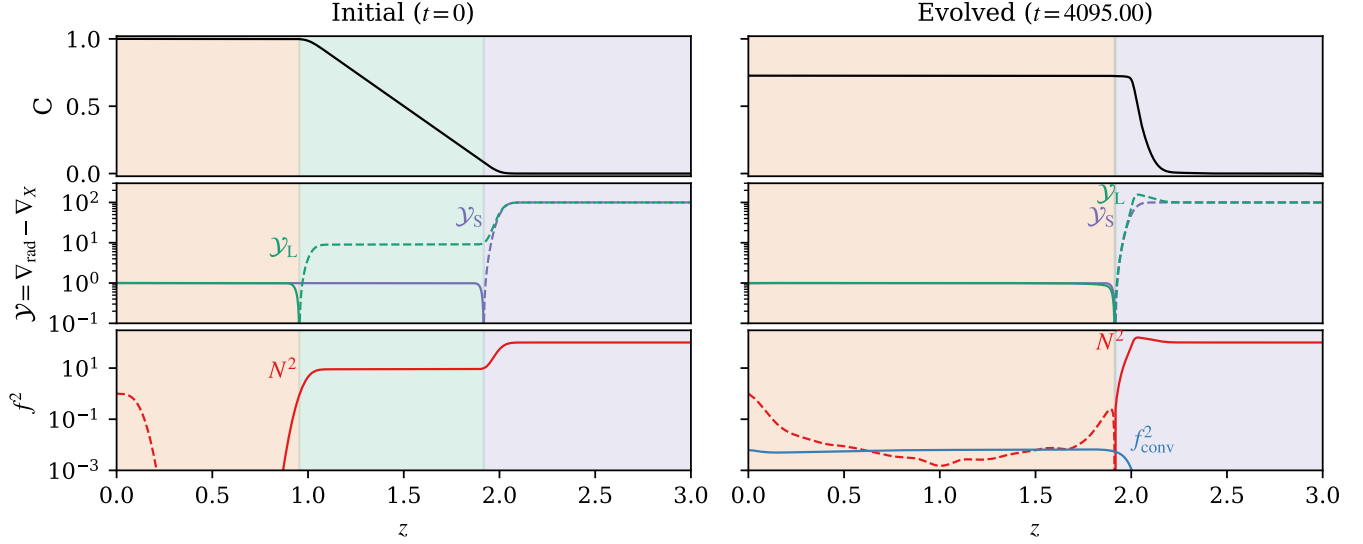


Figure 2. Horizontally-averaged profiles are shown for the composition (top), the discriminants \mathcal{Y}_S and \mathcal{Y}_L (middle, Eqs. 1 & 2), and the Brunt-Väisälä frequency N^2 and the convective frequency $f_{\text{conv}}^2 = |\mathbf{u}|^2 / L_{\text{conv}}$ (bottom), where \mathbf{u} is the velocity and L_{conv} is the depth of the convection zone. Positive values are shown as solid lines and negative values are shown as dashed lines. The initial conditions are shown on the left. The evolved state is shown on the right, where the profiles are averaged over 100 simulation time units. The background is colored so that orange regions are below the zero of \mathcal{Y}_L , green is between the zeros of \mathcal{Y}_L and \mathcal{Y}_S , and purple is above both zeros. While there is a green region in the initial state (Schwarzschild unstable but Ledoux stable), there is no green region in the right state, and the zeros of \mathcal{Y}_L and \mathcal{Y}_S coincide. *Note: this data is taken from a less turbulent run than fig 1; it'll be updated when the fig 1 run finishes.*

the presence of convective flows, but convective boundaries in stars often have $\mathcal{S} \gtrsim 10^6$. The value of \mathcal{S} achieved in these simulations is therefore in the right regime to tell us about stars, but these simulations still exhibit more mechanical overshoot than we would expect stars to.

Finally, In figure 3, we plot a Kippenhahn-like diagram of the simulation. The CZ is shown in orange and is the region below the sign change of both \mathcal{Y}_S and \mathcal{Y}_L . The semiconvection zone is shown in green and is the region below the sign changes of \mathcal{Y}_L and \mathcal{Y}_S . The RZ is shown in purple and is the region above the sign change of both \mathcal{Y}_L and \mathcal{Y}_S . Convection overshoot roughly above the $\mathcal{Y}_L = 0$ line up to the black line, denoted by a hashed region. The height of the black line traces out the region where the vertical profile of the convective kinetic energy falls below 10% of its value in the bulk CZ; this line roughly coincides with the extremum of the composition gradient through the simulation evolution. Importantly, while the orange line that traces out $\mathcal{Y}_L = 0$ and the green line tracing out $\mathcal{Y}_S = 0$ start at different heights, 3D convective motions make these lines converge on long timescales.

4. CONCLUSIONS & DISCUSSION

In this letter, we present 3D simulations of a convection zone and its boundary. The initial boundary is

compositionally stable but weakly thermally unstable (Ledoux stable but Schwarzschild unstable). Entrainment causes the convective boundary to advance until the Ledoux and Schwarzschild criterion agree upon the location of the convective boundary.

These simulations demonstrate that the Ledoux criterion properly defines the *instantaneous* criterion for the boundary of a convection zone. However, when the evolutionary timescale $t_{\text{evolution}} \gg t_{\text{conv}}$, the convective overturn timescale, the Schwarzschild criterion provides the best description of the steady-state boundary of the convection zone. Our 3D dynamical simulations support the claim that “logically consistent” implementations of mixing length theory (Gabriel et al. 2014; Paxton et al. 2018, 2019) must set the Schwarzschild discriminant $\mathcal{Y}_S = 0$ at the convective boundary. This suggests that the MESA software instrument’s modern “convective pre-mixing” (CPM) algorithm should properly find the boundary of most convection zones. Put differently, our simulations suggest that 1D stellar evolution models should not produce different answers when using the Schwarzschild or Ledoux criterion for convective stability when $t_{\text{evolution}} \gg t_{\text{conv}}$.

We note briefly that many Ledoux-stable but Schwarzschild-unstable regions in stars are unstable to overstable doubly-diffusive convection (ODDC). ODDC generally mixes more quickly than the entrainment stud-

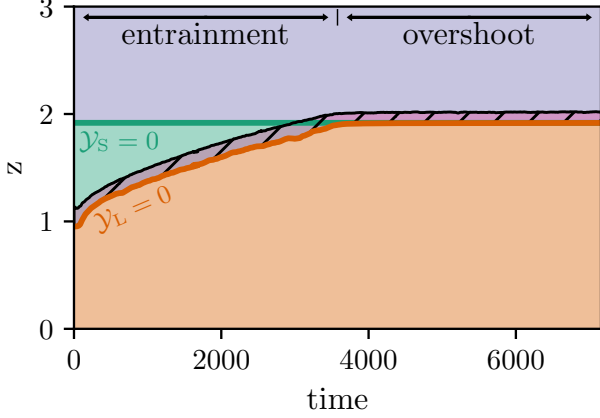


Figure 3. A kippenhahn-like plot of the evolution of our simulation is shown. The orange line traces the Ledoux convective boundary where $\mathcal{Y}_L = 0$, and regions below that are colored orange. The green line traces the Schwarzschild convective boundary where $\mathcal{Y}_S = 0$ and regions below that but above the $\mathcal{Y}_L = 0$ line are colored green. Regions above both lines are colored purple and are stable by both criteria. The black line denotes the location where the kinetic energy falls below 10% of its bulk CZ value; the hashed region below that is an “overshoot zone.” We note that there are two distinct phases in the simulation: an “entrainment” phase when \mathcal{Y}_L advances upwards, and an “overshoot” phase, when \mathcal{Y}_L and \mathcal{Y}_S are steady and convective motions overshoot past them at a constant amount. *Note: this data is taken from a less turbulent run than fig 1; it’ll be updated when the fig 1 run finishes.*

ied here, and has been studied extensively in local simulations (Mirouh et al. 2012; Wood et al. 2013; Xie et al. 2017); see Garaud (2018) for a nice review. ODDC has been applied in 1D stellar evolution models to the regions near main sequence stellar convective cores in Moore & Garaud (2016). They find rapid mixing of ledoux-stable but schwarzschild-unstable regions, and ODDC formulations should be widely included in stellar models.

For stages in stellar evolution where $t_{\text{conv}} \sim t_{\text{evolution}}$, implementations of time-dependent convection (TDC, e.g., Kuhfuss 1986) should be employed to properly capture convective dynamics and the advancement of

convective boundaries. The advancement of convective boundaries in TDC implementations should be informed by time-dependent theories and simulations of the motion of convective boundaries (e.g., Turner 1968; Fuentes & Cumming 2020).

The purpose of this study was to understand how the root of the discriminant \mathcal{Y}_L evolves over time, and whether it coincides with the root of \mathcal{Y}_S at late times. While there is interesting behavior near the boundary beyond that point (e.g., mechanical convective overshoot), a detailed analysis of that phenomenon is beyond the scope of this work. We furthermore constructed the simulations in this work to have a small penetration parameter \mathcal{P} (?) and we see negligible convective penetration in our simulations. Finally, in our simulations, the radiative conductivity is independent of the magnitude of the composition μ , but this is not the case in stars. Since the radiative conductivity sets the location of the Schwarzschild boundary, including these effects would change the exact location of our final convective boundary, but would not change the fundamental takeaways of this work.

In summary, we find that the Schwarzschild criterion provides the location of the convective boundary in a statistically stationary state; in this final state, the Ledoux and Schwarzschild criteria are degenerate.

We thank Meridith Joyce, Anne Thoul, Dominic Bowman, Jared Goldberg, Tim Cunningham, Falk Herwig, Kyle Augustson, (OTHERS?) for useful discussions which helped improve our understanding. EHA is funded as a CIERA Postdoctoral fellow and would like to thank CIERA and Northwestern University. This research was supported in part by the National Science Foundation under Grant No. PHY-1748958, and we acknowledge the hospitality of KITP during the Probes of Transport in Stars Program. Computations were conducted with support from the NASA High End Computing (HEC) Program through the NASA Advanced Supercomputing (NAS) Division at Ames Research Center on Pleiades with allocation GID s2276. The Flatiron Institute is supported by the Simons Foundation.

APPENDIX

A. MODEL & INITIAL CONDITIONS

In this work we study the simplest possible system: incompressible, Boussinesq convection with a composition field and a height-varying background radiative conductivity, similar to that used in Fuentes & Cumming (2020)

and Anders et al. (2021). These equations are

$$\nabla \cdot \mathbf{u} = 0 \quad (\text{A1})$$

$$\partial_t \mathbf{u} + \mathbf{u} \cdot \nabla \mathbf{u} + \nabla \varpi = \left(T - \frac{\mu}{R_0} \right) \hat{z} + \frac{\text{Pr}}{\mathcal{P}} \nabla^2 \mathbf{u}, \quad (\text{A2})$$

$$\partial_t T + \mathbf{u} \cdot \nabla T + w \nabla_{\text{ad}} + \nabla \cdot [-\kappa_{T,0} \nabla \bar{T}] = \frac{1}{\mathcal{P}} \nabla^2 T', \quad (\text{A3})$$

$$\partial_t \mu + \mathbf{u} \cdot \nabla \mu = -\frac{\tau_0}{\mathcal{P}} \nabla^2 \bar{\mu} + \frac{\tau}{\mathcal{P}} \nabla^2 \mu'. \quad (\text{A4})$$

Here, \mathbf{u} is the nondimensional velocity, T is the nondimensional temperature, and μ is the nondimensional concentration. Bars (e.g., \bar{T}) represent the horizontally-averaged component of a field and primes (e.g., T') denote all fluctuations around that background. The nondimensional control parameters are

$$\mathcal{P} = \frac{u_{\text{ff}} L_{\text{conv}}}{\kappa_T}, \quad \text{R}_0 = \frac{|\alpha| \Delta T}{|\beta| \Delta \mu}, \quad (\text{A5})$$

$$\text{Pr} = \frac{\nu}{\kappa_T}, \quad \tau = \frac{\kappa_\mu}{\kappa_T},$$

where the nondimensional freefall velocity is $\mathbf{u}_{\text{ff}} = \sqrt{|\alpha| g L_{\text{conv}} \Delta T}$ with g the constant gravitational acceleration, L_{conv} is the initial depth of the convection zone, $\Delta \mu$ is the composition change across the Ledoux stable region, $\Delta T = L_{\text{conv}}(\partial_z T_{\text{rad}} - \partial_z T_{\text{ad}})$ is the superadiabatic temperature scale of the convection zone, α and β are the coefficients of expansion for T and μ , ν is the viscosity, κ_T is the thermal diffusivity, and κ_μ is the compositional diffusivity. We also specify different values of $\kappa_T = \kappa_{T,0}$ and $\kappa_\mu/\kappa_T = \tau_0$ for the horizontally-averaged component; this allows the radiative gradient to change with height and reduces diffusion on the mean μ structure to ensure evolution is due to advection. These equations are described in detail in Sec. 2 of [Garaud \(2018\)](#), except for the differing diffusivities on the averages and fluctuations.

We define the Ledoux and Schwarzschild discriminants

$$\mathcal{Y}_{\text{S}} = \left(\frac{\partial T}{\partial z} \right)_{\text{rad}} - \left(\frac{\partial T}{\partial z} \right)_{\text{ad}}, \quad \mathcal{Y}_{\text{L}} = \mathcal{Y}_{\text{S}} - \text{R}_0^{-1} \frac{\partial \mu}{\partial z}, \quad (\text{A6})$$

and in this nondimensional system the Brunt-Väisälä frequency is the negative of the Ledoux discriminant $N^2 = -\mathcal{Y}_{\text{L}}$.

In this work, we study a three-layer model in $z = [0, 3]$,

$$\left(\frac{\partial T}{\partial z} \right)_{\text{rad}} = \left(\frac{\partial T}{\partial z} \right)_{\text{ad}} + \begin{cases} -1 & z \leq 2 \\ 10\text{R}_0^{-1} & z > 2 \end{cases}, \quad (\text{A7})$$

$$\frac{\partial \mu_0}{\partial z} = \begin{cases} 0 & z \leq 1 \\ -1 & 1 < z \leq 2 \\ 0 & 2 < z \end{cases}, \quad (\text{A8})$$

where the initial temperature derivative is $\partial T_0/\partial z = (\partial T/\partial z)_{\text{rad}}$ everywhere except between $z = [0.1, 1]$ where it is adiabatic. We set $(\partial T/\partial z)_{\text{ad}} = -1 - 10\text{R}_0^{-1}$.

B. SIMULATION DETAILS & DATA AVAILABILITY

We time-evolve equations A1-A4 using the Dedalus pseudospectral solver ([Burns et al. 2020](#)) using timestepper SBDF2 ([Wang & Ruuth 2008](#)) and safety factor 0.3. All variables are spectral expansions of Chebyshev coefficients in the vertical (z) direction ($n_z = 512$ between $z = [0, 2.25]$ plus $n_z = 64$ between $z = [2.25, 3]$) and as $(n_x, n_y) = (192, 192)$ Fourier coefficients in the horizontally periodic (x, y) directions. Our domain spans $x \in [0, L_x]$, $y \in [0, L_y]$, and $z \in [0, L_z]$ with $L_x = L_y = 4$ and $L_z = 3$. To avoid aliasing errors, we use the 3/2-dealiasing rule in all directions. To start our simulations, we add random noise temperature perturbations with a magnitude of 10^{-6} to the initial temperature profile.

Spectral methods with finite coefficient expansions cannot capture true discontinuities. In order to approximate discontinuous functions such as Eqns. A7 & A8, we define a smooth Heaviside step function centered at $z = z_0$,

$$H(z; z_0, d_w) = \frac{1}{2} \left(1 + \text{erf} \left[\frac{z - z_0}{d_w} \right] \right). \quad (\text{B9})$$

where erf is the error function and we set $d_w = 0.05$. The simulation in this work uses $\mathcal{P} = 3.2 \times 10^3$, $\text{R}_0^{-1} = 10$, $\text{Pr} = \tau = 0.5$, $\tau_0 = 1.5^{-3}$, and $\kappa_{T,0} = \mathcal{P}^{-1}[(\partial T/\partial z)_{\text{rad}}|_{z=0}]/(\partial T/\partial z)_{\text{rad}}$.

We produce figures 2 and 3 using matplotlib ([Hunter 2007](#); [Caswell et al. 2021](#)). We produce figure 1 using plotly ([Inc. 2015](#)) and matplotlib. All of the Python scripts used to run the simulations in this paper and to create the figures in this paper are publicly available in a git repository¹, and in a Zenodo repository (?).

¹ https://github.com/evanhanders/schwarzschild_or_ledoux

REFERENCES

- Anders, E. H., Jermyn, A. S., Lecoanet, D., & Brown, B. P. 2021, arXiv e-prints, arXiv:2110.11356.
<https://arxiv.org/abs/2110.11356>
- Andrassy, R., Herwig, F., Woodward, P., & Ritter, C. 2020, MNRAS, 491, 972, doi: [10.1093/mnras/stz2952](https://doi.org/10.1093/mnras/stz2952)
- Andrassy, R., Higl, J., Mao, H., et al. 2021, arXiv e-prints, arXiv:2111.01165. <https://arxiv.org/abs/2111.01165>
- Basu, S. 2016, Living Reviews in Solar Physics, 13, 2, doi: [10.1007/s41116-016-0003-4](https://doi.org/10.1007/s41116-016-0003-4)
- Basu, S., Verner, G. A., Chaplin, W. J., & Elsworth, Y. 2012, ApJ, 746, 76, doi: [10.1088/0004-637X/746/1/76](https://doi.org/10.1088/0004-637X/746/1/76)
- Burns, K. J., Vasil, G. M., Oishi, J. S., Lecoanet, D., & Brown, B. P. 2020, Physical Review Research, 2, 023068, doi: [10.1103/PhysRevResearch.2.023068](https://doi.org/10.1103/PhysRevResearch.2.023068)
- Carlos, M., Meléndez, J., Spina, L., et al. 2019, MNRAS, 485, 4052, doi: [10.1093/mnras/stz681](https://doi.org/10.1093/mnras/stz681)
- Caswell, T. A., Droettboom, M., Lee, A., et al. 2021, matplotlib/matplotlib: REL: v3.3.4, v3.3.4, Zenodo, doi: [10.5281/zenodo.4475376](https://doi.org/10.5281/zenodo.4475376)
- Claret, A., & Torres, G. 2018, ApJ, 859, 100, doi: [10.3847/1538-4357/aabd35](https://doi.org/10.3847/1538-4357/aabd35)
- Cristini, A., Hirschi, R., Meakin, C., et al. 2019, MNRAS, 484, 4645, doi: [10.1093/mnras/stz312](https://doi.org/10.1093/mnras/stz312)
- Dumont, T., Palacios, A., Charbonnel, C., et al. 2021, A&A, 646, A48, doi: [10.1051/0004-6361/202039515](https://doi.org/10.1051/0004-6361/202039515)
- Farmer, R., Renzo, M., de Mink, S. E., Marchant, P., & Justham, S. 2019, ApJ, 887, 53, doi: [10.3847/1538-4357/ab518b](https://doi.org/10.3847/1538-4357/ab518b)
- Fuentes, J. R., & Cumming, A. 2020, Physical Review Fluids, 5, 124501, doi: [10.1103/PhysRevFluids.5.124501](https://doi.org/10.1103/PhysRevFluids.5.124501)
- Gabriel, M., Noels, A., Montalbán, J., & Miglio, A. 2014, A&A, 569, A63, doi: [10.1051/0004-6361/201423442](https://doi.org/10.1051/0004-6361/201423442)
- Garaud, P. 2018, Annual Review of Fluid Mechanics, 50, 275, doi: [10.1146/annurev-fluid-122316-045234](https://doi.org/10.1146/annurev-fluid-122316-045234)
- Georgy, C., Saio, H., & Meynet, G. 2021, A&A, 650, A128, doi: [10.1051/0004-6361/202040105](https://doi.org/10.1051/0004-6361/202040105)
- Hunter, J. D. 2007, Computing in Science and Engineering, 9, 90, doi: [10.1109/MCSE.2007.55](https://doi.org/10.1109/MCSE.2007.55)
- Inc., P. T. 2015, Collaborative data science, Montreal, QC: Plotly Technologies Inc. <https://plot.ly>
- Jones, S., Andrassy, R., Sandalski, S., et al. 2017, MNRAS, 465, 2991, doi: [10.1093/mnras/stw2783](https://doi.org/10.1093/mnras/stw2783)
- Kaiser, E. A., Hirschi, R., Arnett, W. D., et al. 2020, MNRAS, 496, 1967, doi: [10.1093/mnras/staa1595](https://doi.org/10.1093/mnras/staa1595)
- Kuhfuss, R. 1986, A&A, 160, 116
- Meakin, C. A., & Arnett, D. 2007, ApJ, 667, 448, doi: [10.1086/520318](https://doi.org/10.1086/520318)
- Mehta, A. K., Buonanno, A., Gair, J., et al. 2022, ApJ, 924, 39, doi: [10.3847/1538-4357/ac3130](https://doi.org/10.3847/1538-4357/ac3130)
- Mirouh, G. M., Garaud, P., Stellmach, S., Traxler, A. L., & Wood, T. S. 2012, ApJ, 750, 61, doi: [10.1088/0004-637X/750/1/61](https://doi.org/10.1088/0004-637X/750/1/61)
- Moore, K., & Garaud, P. 2016, ApJ, 817, 54, doi: [10.3847/0004-637X/817/1/54](https://doi.org/10.3847/0004-637X/817/1/54)
- Morrell, S. A. F. 2020, PhD thesis, University of Exeter
- Paxton, B., Cantiello, M., Arras, P., et al. 2013, ApJS, 208, 4, doi: [10.1088/0067-0049/208/1/4](https://doi.org/10.1088/0067-0049/208/1/4)
- Paxton, B., Schwab, J., Bauer, E. B., et al. 2018, ApJS, 234, 34, doi: [10.3847/1538-4365/aaa5a8](https://doi.org/10.3847/1538-4365/aaa5a8)
- Paxton, B., Smolec, R., Schwab, J., et al. 2019, ApJS, 243, 10, doi: [10.3847/1538-4365/ab2241](https://doi.org/10.3847/1538-4365/ab2241)
- Pedersen, M. G., Aerts, C., Pápics, P. I., et al. 2021, arXiv e-prints, arXiv:2105.04533. <https://arxiv.org/abs/2105.04533>
- Pinsonneault, M. 1997, ARA&A, 35, 557, doi: [10.1146/annurev.astro.35.1.557](https://doi.org/10.1146/annurev.astro.35.1.557)
- Salaris, M., & Cassisi, S. 2017, Royal Society Open Science, 4, 170192, doi: [10.1098/rsos.170192](https://doi.org/10.1098/rsos.170192)
- Scott, L. J. A., Hirschi, R., Georgy, C., et al. 2021, MNRAS, 503, 4208, doi: [10.1093/mnras/stab752](https://doi.org/10.1093/mnras/stab752)
- Sestito, P., & Randich, S. 2005, A&A, 442, 615, doi: [10.1051/0004-6361:20053482](https://doi.org/10.1051/0004-6361:20053482)
- Staritsin, E. I. 2013, Astronomy Reports, 57, 380, doi: [10.1134/S1063772913050089](https://doi.org/10.1134/S1063772913050089)
- Turner, J. S. 1968, Journal of Fluid Mechanics, 33, 183, doi: [10.1017/S0022112068002442](https://doi.org/10.1017/S0022112068002442)
- Viani, L. S., & Basu, S. 2020, ApJ, 904, 22, doi: [10.3847/1538-4357/abba17](https://doi.org/10.3847/1538-4357/abba17)
- Wang, D., & Ruuth, S. J. 2008, Journal of Computational Mathematics, 26, 838. <http://www.jstor.org/stable/43693484>
- Wood, T. S., Garaud, P., & Stellmach, S. 2013, ApJ, 768, 157, doi: [10.1088/0004-637X/768/2/157](https://doi.org/10.1088/0004-637X/768/2/157)
- Woodward, P. R., Herwig, F., & Lin, P.-H. 2015, ApJ, 798, 49, doi: [10.1088/0004-637X/798/1/49](https://doi.org/10.1088/0004-637X/798/1/49)
- Xie, J.-H., Miquel, B., Julien, K., & Knobloch, E. 2017, Fluids, 2, doi: [10.3390/fluids2010006](https://doi.org/10.3390/fluids2010006)